DSP-based Inter-Channel Interference Monitoring in Flexible Wavelength Routed Networks

*To be published in Journal of Optical Communications and Networking:*

**Title:** DSP-based Inter-Channel Interference Monitoring in Flexible Wavelength Routed Networks

**Authors:** Leonardo Minelli,Gabriella Bosco,Stefano Straullu,Antonino Nespola,Stefano Piciaccia,Dario Pilori

**Accepted:** 14 May 24

**Posted** 14 May 24

**DOI:** https://doi.org/10.1364/JOCN.523440

# DSP-based Inter-Channel Interference Monitoring in Flexible Wavelength-Routed Networks

LEONARDO MINELLI[1,*], GABRIELLA BOSCO[1], STEFANO STRAULLU[2], ANTONINO NESPOLA[2], STEFANO PICIACCIA[3], AND DARIO PILORI[1]

[1] DET, Politecnico di Torino, C.so Duca degli Abruzzi 24, Torino, Italy
[2] LINKS Foundation, Via Pier Carlo Boggio 61, Torino, Italy
[3] Cisco Photonics Italy S.r.l., Via Santa Maria Molgora 48/C, Vimercate, Italy
[*] leonardo.minelli@polito.it

*Compiled May 14, 2024*

**The efficiency of optical networks employing flexible wavelength division multiplexing (WDM) can be increased by maximizing the throughput of each individual channel, provided that the position of its neighboring channel is known with sufficient accuracy in order to avoid inter-channel interference. In this manuscript, we propose a digital signal processing (DSP) algorithm, leveraging the use of an artificial neural network (ANN), to estimate the neighboring channels distance by processing raw digital samples from a standard coherent receiver. We present an efficient dataset design approach, based on latin hypercube sampling (LHS), in order to effectively optimize and validate the algorithm under different assumptions on the optical WDM channels. We investigate the accuracy of the ANN-based DSP scheme through simulation analysis, highlighting its potential in relation to the characteristics of the optical network. Finally, we validate our approach in an experimental setup using standard commercial coherent transceivers. The experimental results show that the distance from the neighboring WDM channels can be estimated with a Root Mean Square Error (RMSE) of less than 1.5 GHz for a channel under test with symbol rate of 52 GBaud.**

http://dx.doi.org/10.1364/ao.XX.XXXXXX



## 1. INTRODUCTION

To cope with the 40-60% compound annual growth rate (CAGR) of internet traffic [1], modern optical networks need to be continuously upgraded. While for short-reach systems this can be obtained by deploying new fiber pairs [2, 3], for long-distance networks the cost of deploying new fiber is usually prohibitive. Consequently, the preferable solution is the maximization of the throughput of the currently deployed fiber networks. This can be achieved in different ways, such as deploying Ultra-Wide-Band (UWB) systems [4, 5] or using advanced DSP techniques, such as Probabilistic Constellation Shaping (PCS) [6, 7], to increase the spectral efficiency, up to the fiber capacity [8]. These techniques can be used either to increase the capacity of the network, or to provide reach extension at the same data-rate. However, the capacity can also be increased by improving the network's *efficiency*, e.g. by better exploiting the already available optical spectrum. In fact, thanks to flexible technologies, the use of a flexible Wavelength Division Multiplexing (WDM) grid, combined with a tightly-spaced channel allocation can give significant benefits to the network [9]. Moreover, a flexible use of the spectrum can be combined with advanced DSP techniques (e.g. PCS), to provide additional degrees of freedom at the link design level for network optimization.

In [10] the authors demonstrated a network throughput benefit by increasing the symbol rate of each individual WDM channel according to the available bandwidth. Obviously, this requires that the transceivers support such functionality, and that the network can be dynamically reconfigured to support this adjustment. The available bandwidth either depends on the filtering of the Reconfigurable Optical Add-Drop Multiplexers (ROADMs), or, especially in the context of filterless optical networks [11], on the position of the neighboring WDM channels. In the latter case, the operation is feasible only if the position of the neighboring WDM channels is accurately known, which allows the estimation and the computation of the Inter-Channel Interference (ICI) penalty. For instance, internal Cisco guidelines recommend a spectral separation between channels not smaller than 9% for BPSK/QPSK, and $10-15\%$ for larger constellations, compared to the symbol rate.

However, in the context of modern, multi-vendor, open and disaggregated optical networks [12], this information may not be readily available at the receiver. Moreover, while it can be measured by using external hardware, such as high-resolution

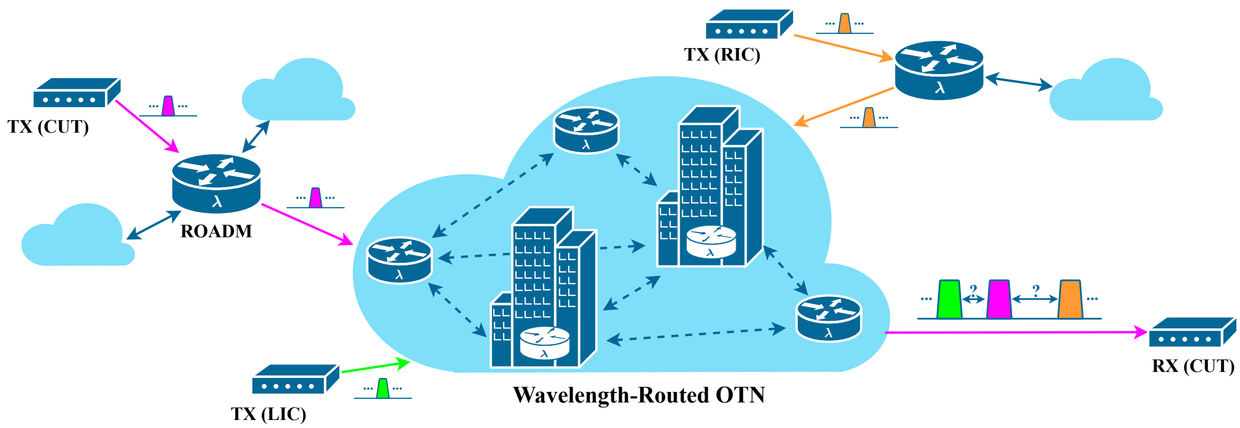


**Fig. 1.** High-level scheme of the transmission of a WDM channel under test (CUT) through an flexible Wavelenength-Routed Optical Transport Network (OTN). The signal, while being propagated from the Transmitter (TX) to the Receiver (RX), is forwarder through several ROADM, which may randomly append in the WDM comb a Left-interfering Channel (LIC) and/or a Right Interfering Channel (RIC), with unknown frequency spacing from the CUT.

Optical Spectrum Analyzers (OSAs), a widespread use of such devices in the network can be expensive. Therefore, a better approach is the exploitation of simple Digital Signal Processing (DSP) algorithms, that can be implemented in standard coherent receivers, to estimate the position of the neighboring WDM channels, and, thus, the amount of ICI.

Different methods have already been proposed to estimate the position of unfiltered neighboring WDM channels, e.g. by using the equalizer coefficients [13] or the constellation points [14–16]. However, the performance of these methods may be affected by the specific DSP chain implemented in the receiver. Moreover, they lack the ability to estimate the precise location (i.e., left/right in the spectrum) of the interfering channels.

In this work, extending [17], we propose a novel Artificial Neural Network (ANN)-based DSP estimation scheme for the estimation of the position of the neighboring WDM channels. The algorithm is based on processing the spectrum of the raw samples captured by the Analog-to-Digital Converter (ADC) of a coherent receiver. Therefore, it can be easily implemented in existing receivers, for instance using an external board that periodically performs an off-line processing, or by integrating it with timing recovery algorithms, since they are usually based on band-pass filtering of ADC samples along the spectral edges [18]. This scheme is robust also to strong ROADM filtering, albeit with lower accuracy for distanced channels. The algorithm is first tested over extensive simulative scenarios to assess its capabilities and limitations in a tightly controlled setup. Then, the algorithm is validated in an experimental demonstration using a commercial coherent receiver at 52 GBaud, showing that the position of the neighboring WDM channels can be estimated with a Root Mean Square Error (RMSE) of less than 1.5 GHz (i.e., approximately 2.9% of the CUT symbol rate).

## 2. SCENARIO AND METHODOLOGY

### A. System scenario

We assume a modern optical network, built on a flexible WDM grid [9], as shown in Fig.1, considering only a single lightpath in the network. An example of Received Optical Spectrum (ROS) is shown in Fig.2. The lightpath's channel (Channel Under Test - CUT) is conventionally put at the center of the spectrum ($f = 0$), with a symbol rate equal to $R_s$ and a roll-off (assuming a root

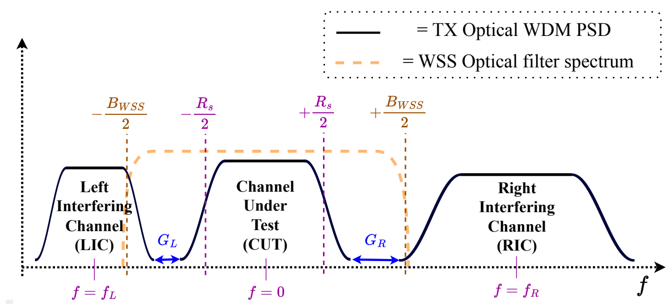


**Fig. 2.** Received Optical Spectrum (ROS) at the receiver under test. The CUT is conventionally at $f = 0$, and the two interfering WDM channels are shown at the left and at the right of the CUT. The guard-bands $G_L$ and $G_R$ are shown, along with the central frequencies of the channels. Optionally, a WSS with bandwidth $B_{\text{WSS}}$ centered at the CUT can be placed before the receiver.

raised cosine shaping filter) equal to $\rho$. The two neighboring WDM channels are shown at the two edges of the spectrum. The Left Interfering Channel (LIC) and the Right Interfering Channel (RIC) are centered at $f_L < 0$ and $f_R > 0$, with symbol rate $R_{s,L}$ and $R_{s,R}$ and roll-off $\rho_L$ and $\rho_R$, respectively. Their power, as it is measured at the receiver of the CUT, is $P_L$ and $P_R$. While, usually, the power of all the channels is equalized in the network, for this work we assume a general case where the power might be potentially different. Moreover, the LIC and the RIC are assumed to be generated in any part of the network: therefore, their transmission parameters may be only partially or even completely unknown at the receiver.

The main goal of this work is the estimation of the *guard-band*, $G_L$ and $G_R$, which unambiguously defines the spectral separation between the CUT and the LIC and RIC, respectively, considering the end of the spectral support of each channel:

$$G_L = f_L + \frac{R_{s,L}(1+\rho_L) + R_s(1+\rho)}{2} \quad \text{(1)}$$

$$G_R = f_R - \frac{R_{s,R}(1+\rho_R) + R_s(1+\rho)}{2} \quad \text{(2)}$$

This value of guard-band can be then used to optimize the sym-

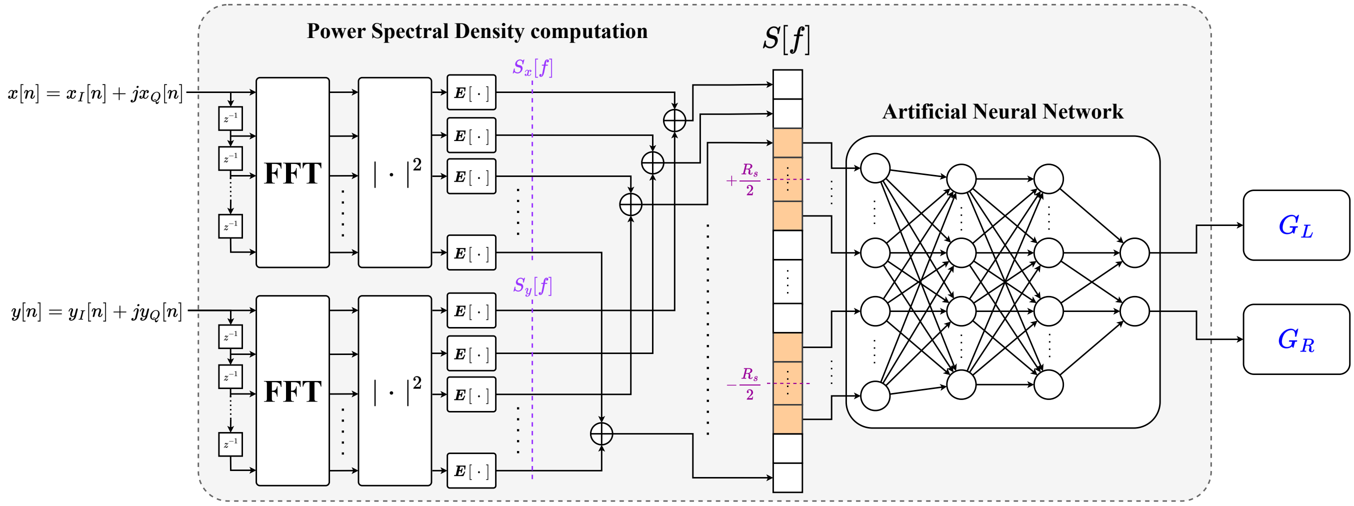


**Fig. 3.** Block scheme of the proposed DSP scheme for ICI monitoring through guard-band estimation.

bol rate of the CUT $R_s$, thus increasing the CUT's throughput [10]. After estimating both guard-bands, the CUT symbol rate can be indeed varied by $\Delta R_s = 2/(1+\rho) \cdot min\,(G_L, G_R) - \mu$, where $\mu$ is a positive safety margin term accounting for the algorithm estimation uncertainty[1].

Optionally, we can assume optical filtering is present in the network, e.g. introduced by Wavelength Selective Switches (WSSs), whose bandwidth is denoted as $B_{WSS}$ in Fig.2. The WSS filtering is assumed to be centered on the CUT, while the bandwidth is assumed to be generally greater than that of the channel ($B_{WSS} > R_s \cdot (1+\rho)$). This optical filtering induces two main effects. Firstly, it may act as a constraint on the maximum tolerable symbol rate of the CUT. Secondly, it reduces the accuracy of the estimation of LIC and RIC positions. In this work, we focus only on the second effect, without considering the additional constraint on the maximum symbol rate. Interested readers may refer to specific works, such as [19–21], for the transmission impairments on the CUT induced by tight WSS filtering in optical networks.

### B. Guard-band estimation ANN-based DSP scheme

A high level overview of the proposed DSP scheme is shown in Fig.3. The proposed ANN-based DSP algorithm estimates the guard-bands $G_L$ and $G_R$ by exploiting, as input feature, the received discrete sequence captured by the ADC of a standard coherent receiver [22]. The received samples, on both polarizations using the Jones notation, can be expressed as

$$\begin{cases} x[n] = x_I[n] + jx_Q[n] \\ y[n] = y_I[n] + jy_Q[n] \end{cases} \tag{3}$$

where $X$ and $Y$ are the two polarizations, $I$ and $Q$ are the In-Phase and Quadrature components, and $n$ is the discrete time index.

A single $G_L$ and $G_R$ estimate requires two main DSP steps (see Fig.3). First, the DSP scheme evaluates the discrete dual-polarization Power Spectral Density (PSD) of the received signal $S[f]$ (where $f$ is the frequency), defined as

$$\begin{aligned} S[f] = S_x[f] + S_y[f] = |X[f]|^2 + |Y[f]|^2 = \\ = \begin{pmatrix} X[f] & Y[f] \end{pmatrix} \cdot \begin{pmatrix} X[f] \\ Y[f] \end{pmatrix}^* \end{aligned} \tag{4}$$

where $S_x[f] = |X[f]|^2$ and $S_y[f] = |Y[f]|^2$ are the PSDs over the $X$ and $Y$ polarizations, estimated by computing the absolute squared values of the Discrete Fourier Transforms (DFT) for the $x[n]$ and $y[n]$ sequences, respectively. Specifically, the two PSDs are estimated following the Bartlett's periodogram estimation method, i.e., by averaging the squared modulus of successive Fast Fourier Transform (FFT) evaluations of the discrete signals [23]. The PSDs were estimated over 2048 consecutive ADC samples using an FFT window of 256 samples. The obtained dual-polarization PSD constitutes an efficient representation of the WDM channel status when exploiting the RX ADC samples, since it preserves the spectral content of the received signal, and it is immune not only to phase-only effects such as Chromatic Dispersion (CD) and phase noise, but also to Polarization Mode Dispersion (PMD). The latter property can be verified by the following equality:

$$\begin{aligned} \begin{pmatrix} X[f] & Y[f] \end{pmatrix} \cdot \begin{pmatrix} X[f] \\ Y[f] \end{pmatrix}^* = \\ = \left( \begin{pmatrix} X[f] & Y[f] \end{pmatrix} \cdot \mathbf{U}[f]^\top \right) \cdot \left( \mathbf{U}[f] \cdot \begin{pmatrix} X[f] \\ Y[f] \end{pmatrix} \right)^* \end{aligned} \tag{5}$$

where $\mathbf{U}[f]$ is an arbitrary unitary matrix.

Consequently, the vector $S[f]$ is then used as an input for an Artificial Neural Network (ANN), which jointly estimates the guard-band values $G_L$ and $G_R$. The adopted ANN architecture adheres to the standard Feed-Forward Neural Network (FFNN) structure (as in [16]). The adopted configuration features 2 hidden layers, positioned between the input features and the output layer. Each hidden layer is composed by 25 neurons, which utilize the Leaky-ReLU activation function. The output layer is composed instead by 2 linear layers (i.e., no activation

[1] E.g. we can define $\mu = 3 \cdot RMSE$ according to a $3\sigma$ empirical rule, assuming the estimation error to be Gaussian.

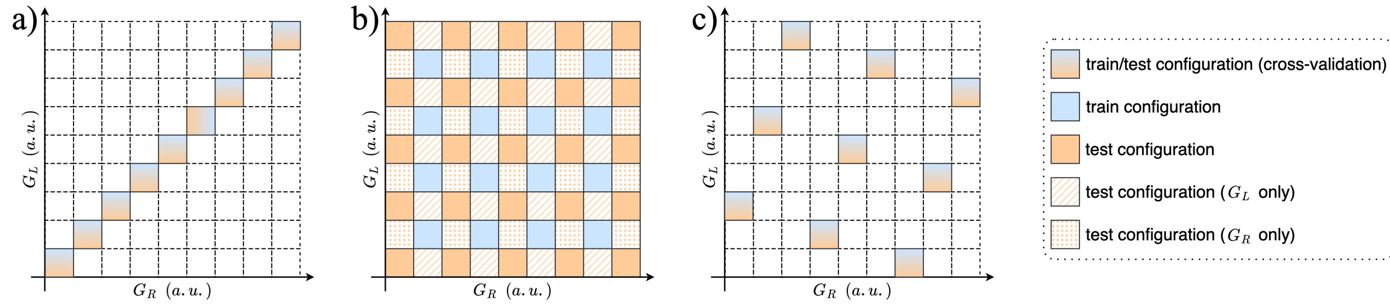


**Fig. 4.** Different Sampling Strategies for Guard-band Dataset design: a) Symmetric Guard-band value sampling; b) Grid-based sampling; c) Optimal Latin Hypercube based sampling. Square color and filling pattern specify the usage for the sampled $G_L$ and $G_R$ values, as specified in the legend (right).

function), in order provide the guard-band estimate for both the LIC and the RIC jointly. The complexity of the architecture has been selected consistently with the FFNN adopted in our previous work [16].

#### *B.1. Integration of the proposed scheme within coherent transceivers*

In standard coherent transceivers, the same FFT samples used by the proposed algorithm are typically already computed within the receiver's DSP chain. Specifically, FFT-based timing error detection (TED) schemes [24], such as the Godard System [25], extract from both polarizations a selected window of the signal spectrum, centered around half of the transmission symbol-rate. Consequently, in this work, the PSD computation is specifically confined to two distinct spectral regions, encompassing 110 consecutive frequency bins and centered around half of the CUT symbol rate, denoted as $f = \pm R_s/2$ (orange entries of $S[f]$ in Fig.3), in order to make our algorithm potentially compatible with such schemes (i.e., by extracting the PSD information directly from the TED inner signals). Moreover, the use of these spectral regions reduces the computations required for the Bartlett periodogram, and diminishes the number of input features to the FFNN (220 instead of 256).

### C. Latin Hypercube sampling dataset design

In this work, we merely adopted a standard FFNN architecture without focusing on the development of the DSP scheme by optimizing the ANN structural hyperparameters. Given the fast evolving landscape in the Deep Learning research [26], various promising ANN architectures are currently being discovered, developed and investigated. Consequently, the detailed refinement and optimization of a specific ANN architecture tailored for guard-band estimation is outside the scope of this work. In this study, we focused instead on the design of an appropriate dataset to effectively optimize and then validate the neural network performance, which in the context of a flexible wavelength-routed optical network requires significant attention. Specifically, we were interested in designing an appropriate set of WDM channel configurations, from which acquiring the required RX ADC samples to be given in input to the proposed ANN-based DSP scheme for guard-band estimation. When using supervised learning approaches (i.e., neural nets) to this end, the following aspects must be indeed jointly considered:

**Limited Dataset size** Due to practical resource constraints, relative to the algorithm implementation using a commercial transceiver, the dataset must be acquired from a limited set of experimental configurations of the WDM network;

**Realistic Assumptions on WDM Channel** To robustly operate in a realistic flexible WDM scenario, the ANN-based algorithm needs to be trained on a dataset designed with assumptions effectively representing the target optical network behavior. Among them, assumptions on the CUT parameters can be rigid without practical consequences: different ANN coefficient configurations can be deployed within the optical transceiver depending on the CUT operative point. Conversely, assumptions on the LIC and RIC parameters (e.g., guard-band from CUT, roll-off, symbol rate, OSNR, etc.) are required to be sufficiently wide in order to encompass reliably a dynamic WDM channel in a flexible optical network;

**Even coverage of the interfering channels parameters space** The parameters of the WDM channel need to be uniformly and independently varied as much as possible throughout the entire dataset, in order to prevent lack of generalization of the algorithm: the latter would indeed lead to overfitting, when training and evaluating the performance of the ANN-based scheme. Specifically to the joint left and right guard-band estimation, the parameters independence involves an asymmetric variation of the LIC and RIC configuration within the dataset.

The illustrated requirements significantly differ from the approach followed in our previous work, where the frequency spacing between the CUT and the interfering channel was kept symmetric [16]: as an example, Fig.4 compares the different strategies for sampling $G_L$ and $G_R$ values during dataset design, targeting the sampling of a maximum total of $N = 9$ configurations for the WDM channel.

When the dataset is designed to have symmetrically spaced LIC and RIC[2] (Fig.4.a), it is straightforward to sample $N$ uniformly distributed values for both $G_L$ and $G_R$. $N$ configurations of the WDM channel are indeed sufficient to create the dataset (equivalently to what done in [16]), and cross-validation can be seamlessly applied on the dataset to efficiently train and test the ANN, for instance by applying $k$-folding on the configurations [27]. Conversely, when varying independently $G_L$ and $G_R$, the asymmetry poses some challenges. A first intuitive approach might be to sample both $G_L$ and $G_R$ values in a grid-based fashion, as illustrated in Fig.4.b. This approach, however, badly scales with the dataset size: $N^2$ configurations would be

[2]For simplicity, we neglect here the variation of other parameters of the LIC and RIC.

required to just sample $N$ values of each guard-band or, by induction, $N^{2M}$ configurations would be needed if considering to vary $M$ free parameters for each interfering channel. Moreover, a grid-based approach would lead to inefficient dataset splitting for training and testing the Neural Network, as the $G_L$ and $G_R$ values within the training dataset cannot be present also in the test dataset (in order to avoid performance overestimation due to overfitting). As shown in the example in Fig. 4.b only small percentages of the dataset could be actually exploited for training the ANN (even with sole guard-bands variation), and cross-validation would be not feasible (as in the simplified symmetric scenario depicted in Fig. 4.a).

To overcome this issue, in this work, we propose to design the dataset by varying the free-parameters of the WDM channel a using Latin Hypercube Sampling (LHS) [28] approach. The Latin Hypercube is a multidimensional generalization to the Latin Square. In the statistical sampling context, the latter consists of a 2-dimensional grid, containing uniformly varied sampling positions characterized to be unique for each row and column: Fig. 4.c illustrates the optimal application of LHS for sampling $N = 9$ configurations of $G_L$ and $G_R$ values. Using an LHS approach, a dataset can be designed with a size that properly scales with the number of $M$ free interfering channel parameters: by just acquiring the dataset from $N$ configurations, each parameter is systematically varied across $N$ uniformly distinct values throughout the entire dataset, independently from the others. Moreover, LHS ensures that each configuration within the dataset is uniquely characterized by a distinct set of parameter values, eliminating repetitions across all configurations. This enables the use of cross-validation techniques over the the dataset configurations without the concern of overfitting. Consequently, a dataset designed with LHS guarantees an efficient usage of the (typically limited) available data during both training and testing of the algorithm.

In practice, multiple LHS realizations exist for a given number of free parameters and configurations. Therefore, to ensure an even coverage of the parameter space, the LHS process can be optimized in order to incorporate the desired statistical properties (such as those of orthogonal sampling, a particular case of LHS [29]). In the following sections, for both simulations and experiments the WDM channel parameters are varied using LHS, optimized by means of a minimum correlation criterion, adopting MATLAB® `lhsdesign()` implementation.

## 3. ACCURACY OF THE ALGORITHM

### A. Simulation setup

As discussed in Sec.2-A, the LIC and the RIC can be transmitted at any point in the optical network. This means that the receiver of the CUT might not have full knowledge of their parameters (e.g. symbol rate, roll-off, ...). Consequently, the accuracy of the estimation algorithm can be significantly affected by the degree of knowledge of the parameters. For this reason, before the experimental validation, we executed an extensive set of numerical simulations, to assess the maximum accuracy obtainable by the algorithm, at different degrees of knowledge on the interfering channels. The simulation setup is described in Fig.5. Three independent transmitters generate three WDM channels, modulated with PM-16-QAM and shaped with a root-raised-cosine filter.

Following the notation of Fig.2, each channel has a potentially different central frequency, roll-off, symbol rate and received power. Then, ASE noise is inserted, to set a given OSNR at the receiver, followed by an optional optical filtering by a WSS, modeled as in [30]. The receiver is modeled as a simple downsampler at 2 samples per symbol (SPS), preceded by an ideal anti-aliasing filter: this emulates an optimal coherent receiver followed by 4 ideal ADCs. Since the goal of this section is a mere study on the accuracy of the algorithm for different degrees of knowledge of the interferers, the simulation setup is purposefully very simple and ideal. The effects of impairments induced by realistic receivers will be assessed in the experimental demonstration, described in the next Section.

| Case # | LIC and RIC parameters | | |
|---|---|---|---|
| | $P_{L/R}$ | $\rho_{L/R}$ | $R_{s,L/R}$ |
| 1 | fixed | fixed | fixed |
| 2 | variable | fixed | fixed |
| 3 | fixed | variable | fixed |
| 4 | fixed | fixed | variable |
| 5 | variable | variable | fixed |
| 6 | variable | fixed | variable |
| 7 | fixed | variable | variable |
| 8 | variable | variable | variable |

**Table 1.** Parameters of the interfering channels in the different simulation cases.

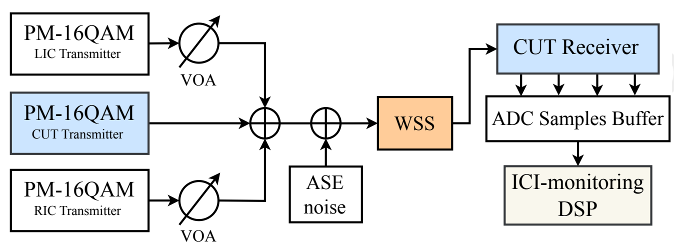


**Fig. 5.** Simulated guard-band estimation setup.

We designed 8 different simulation cases, detailed in Table 1. For each case, concerning the left and right interfering channels parameters, we kept the power ($P_{L/R}$), the symbol rate ($R_{s,L/R}$) and the roll-off ($\rho_{L/R}$) either fixed (i.e. constant) or variable. This approach enabled us to explore various degrees of knowledge of the interferers at the receiver without changing the algorithm structure, which relies solely on the ADC samples as input features. In each case, we designed 900 different WDM channel configurations, where the free parameters of the interfering channels were swept according to LHS with an emphasis on minimizing correlation [28]. For each configuration, we simulated the transmission and acquisition from the CUT receiver of $2^{17}$ consecutive ADC samples (X/Y polarization and I/Q phase). Then, training and test of the ANN-based DSP were performed through $k$-folding over the acquisition configurations, with $k$ factor set to 10. For each fold, the neural network training process involved a standard Stochastic Gradient Descent (SGD) approach, where random batches of ADC samples were iteratively forwarded and backward propagated through the ANN-based DSP scheme, repeating the procedure for 50,000 times. Specifically, within each iteration, $60 \times 4 \times 2048$ consecutive ADC samples were drawn randomly from the training

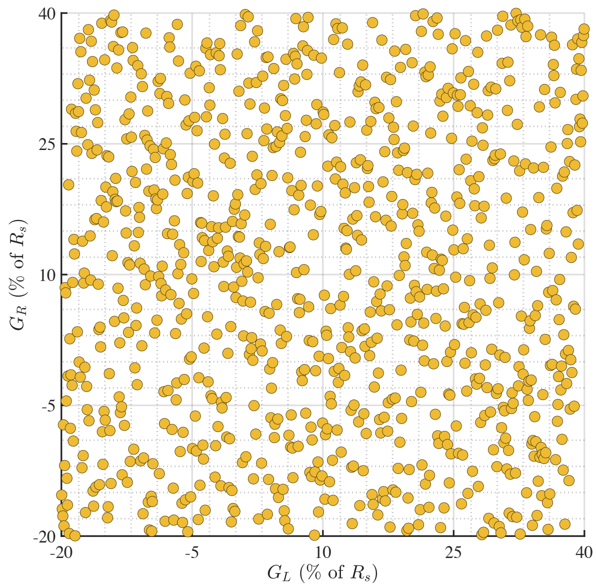


**Fig. 6.** Latin Hypercube sampling of the Guard-band values for the simulation case #1.

dataset, with 60 representing the batch size and 4 corresponding to the X/Y and I/Q components. Throughout each iteration, the Mean Square Error (MSE) loss gradient back-propagation was deployed to update the ANN coefficients through SGD. The latter was implemented utilizing the Adam optimization, with learning rate set to $\epsilon = 0.001$ and first and second moment parameters set respectively to $\beta_1 = 0.9$ and $\beta_2 = 0.999$.

The parameters of the CUT were kept fixed (as motivated in Section 2.C), with a roll-off $\rho$ set to 0.2 and a nominal OSNR (assuming no interfering channels) set to 17 dB. The symbol rate of the CUT $R_s$ is assumed to have arbitrary value, yet relative to the simulation of received ADC samples at 2 SPS. The parameters of the interfering channels were swept according to the following criteria. The LIC/RIC roll-off $\rho_{L/R}$ was either kept fixed to 0.2 as for the CUT, or varied between 0.1 and 0.3, the power at the CUT receiver was either kept fixed to 0 dB or varied between $\pm 3$ dB with respect to the CUT power, and the symbol rate $R_{s,L/R}$ was either kept equal to $R_s$ or varied between 0.50 and 1.50 times the CUT symbol rate. The guard band values $G_{L/R}$ were varied consistently to the roll-off and symbol rate, with minimum and maximum values defined as in Eq. (6) and Eq. (7).

$$G_{L/R,\min} = -\frac{\max(\rho_{L/R}) \cdot \max(R_{s,L/R}) + \rho \cdot R_s}{2} \quad \textbf{(6)}$$

$$G_{L/R,\max} = \frac{R_s}{2}\,(1 - \rho) \quad \textbf{(7)}$$

Specifically, the minimum guard-band value is relative to a worst-case configuration of the WDM channel where the 3-dB bandwidth of the CUT and the widest interfering channel overlap, while the maximum value is relative to the largest frequency distance from the CUT that an interfering channel can have while still being observable within a 2-SPS ADC samples spectrum.

An example of the simulated values of guard-band $G_L$ and $G_R$ for the case #1 is shown in Fig.6. In this case, as the roll-off and the symbol rate of the interfering channel are fixed, the variation of $G_L$ and $G_R$ is caused only by the relative variation of the central frequencies ($f_L$ and $f_R$), according to LHS. Similar relative distribution of guard-band was obtained in the other simulation cases, but not identical, as in those scenarios the LHS was optimized to minimize the correlation also with respect to the other interfering channels free parameters.

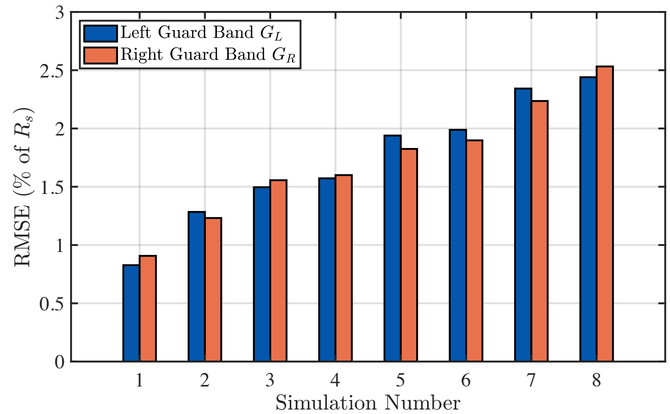


**Fig. 7.** Simulation results, shown in terms of Root Mean Square Error (RMSE) of the estimated left guard-band (blue bars) and right guard-bands (orange bars) in the simulation cases detailed in Table 1. No optical filtering was applied at the receiver.

### B. Simulation Results

The performance of the proposed algorithm is first evaluated in terms of Root Mean Square Error (RMSE) between the estimated and true value of the left and right guard-bands. Fig.7 shows the simulation results by comparing the RMSE performances across the different simulation cases detailed in Table 1 without applying any optical filtering at the receiver (i.e., adopting the setup shown in Fig.5 assuming an ideal WSS).

The results clearly indicate that the accuracy of the algorithm is influenced by the degree of knowledge about the interfering channels. For instance, for the case #1 (all free parameters fixed), the RMSE of the estimation of the guard-band is less than 1% of the symbol rate; on the contrary, for the case #8 (all free parameters variable and unknown to the algorithm) the RMSE is greater, approximately 2.5%. Assuming a symbol rate of 52 GBaud (as in the experiments illustrated in Sec.4), this corresponds to an RMSE degradation from 0.4 GHz to 1.3 GHz. Moreover, it is noteworthy that the RMSE performances of simulation cases #3 and #5 (variable roll-off, fixed symbol rate) closely mirror the performances of cases #4 and #6 (fixed roll-off, variable symbol rate). The correlation of results is expected, since, within the frequency domain of the CUT RX samples spectrum $S[f]$, the spectral segments relative to interfering channels with roll-off from 0.1 to 0.3 vary identically to those of LIC and RIC with symbol rate varying from 0.5 to 1.5 times the CUT rate $R_s$.

As a further performance analysis, simulations were re-run by introducing the effects of a WSS at the receiver (as shown in Fig.5), which partially filters the LIC and RIC. As discussed in the Introduction, the WSS reduces the available bandwidth for the CUT, and at the same time can reduce the estimation accuracy of the algorithm. Therefore, we tested the algorithm by introducing a WSS at the receiver, modeled according to [30], with a $B_{\mathrm{OTF}}$ equal to 0.2 times the CUT symbol rate, and a 3-dB bandwidth ranging from the symbol rate of the CUT up to 1.5 times the symbol rate. The results relative to the application of the WSS in the simulation case #8 are shown in Fig.8: the perfor-

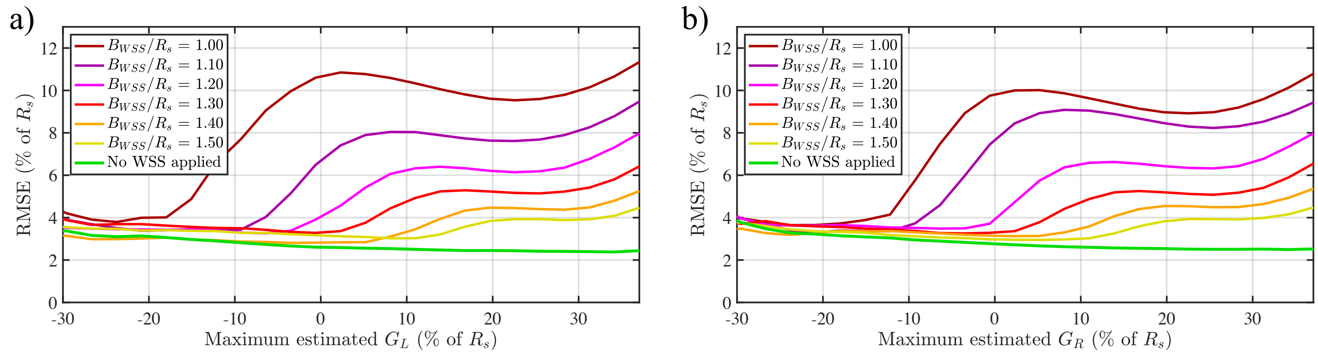


**Fig. 8.** Simulation results, shown as RMSE of the estimated left (a) and right (b) guard-band, for the case #8, as a function of the maximum guard-band, for different values of WSS filtering.

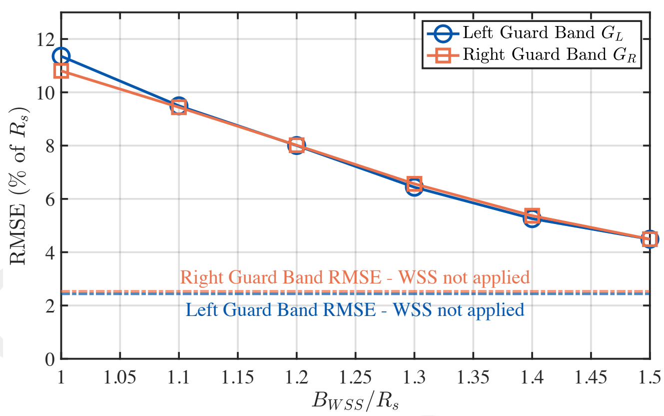


**Fig. 9.** Overall RMSE performance for left and right guard-band estimation for the simulation case #8, as a function of the WSS bandwidth.



mance is shown in term of RMSE of the estimation of the guard-bands (left and right), displayed as function of the maximum estimated guard-band and the optical filter bandwidth. From the Figure, it is clear that, when the estimated guard-bands are lower than the difference between the WSS bandwidth ($B_{WSS}$) and that of the CUT ($R_s(1+\rho)$), the RMSE is around 4%. Its value in this region tends to increase as $B_{WSS}$ is lower; nevertheless, the performance remains comparable to the case in which no WSS is applied (green lines in Fig.8). However, the estimation error becomes significantly larger as soon as the algorithm attempts estimating higher guard-bands: those values are indeed relative to significantly distanced interfering channels, whose information in the received signal is entirely filtered out by the WSS. Consequently, the algorithm maintains precision within a guard-band range that contracts proportionally to the decrease of the optical filter bandwidth $B_{WSS}$. Finally, Fig.9 shows the overall RMSE when the algorithm estimates all the simulated guard-band values, as a function of the WSS bandwidth. It is clear from the plot that the accuracy of the algorithm decreases as the bandwidth of the WSS is lower. Nevertheless, the lack of accuracy for low $B_{WSS}$ values is not practically relevant, since in such cases the maximum symbol rate of the CUT would be indeed limited only by the WSS, and not by interfering channels. Thus, the guard-band would be an useless parameter for the purpose of the CUT symbol rate maximization.

### C. Discussion on simulation results

From the extensive simulation campaign, albeit in a simplified and ideal scenario, two main conclusions can be drawn. First, the inherent accuracy of the algorithm is below 1% of the symbol rate of the CUT, which is the accuracy obtained when only the guard-bands are unknown. If other characteristics (such as symbol rate, roll-off or relative power) of the interfering channels are also unknown, the accuracy diminishes. Nevertheless, it remains within an acceptable range for the intended application. Second, in the presence of optical filtering which (at least partially) filters out information about the interferers, the accuracy is reduced. However, if the WSS bandwidth is sufficiently large compared to the guard-band range under monitoring[3], the algorithm precision remains acceptable: this is a crucial finding, as it represent the only scenario where the estimation of the guard-band is useful for the purpose of increasing the symbol rate of the CUT.

In summary, across all the simulative cases, we can conclude that this approach is viable. This means that the guard-band can be estimated with a sufficient accuracy to increase the symbol rate of the CUT to maximize the usage of the available optical bandwidth, thus increasing the efficiency of the entire network. A validation of the algorithm in a realistic scenario, which has been carried out through experiments deploying commercial coherent transceivers, is then described in the next Section.

## 4. EXPERIMENTAL VALIDATION OF THE ALGORITHM

### A. Experimental Setup

The experimental setup is shown in Fig.10(a), and it was set to closely mimic the simulation setup of the previous section. During the experiments, three commercial transmitters (CISCO NCS-1004) generated the three WDM channels relative the CUT and the two interfering channels, the LIC and the RIC. The three channels were combined using a coupler, and optionally filtered by a WSS (Finisar WaveShaper), with $B_{OTF}$ close to 10 GHz. The experimental setup was deployed to acquire a dataset for the algorithm relative to five different scenarios: one in which optical filtering was not applied, and four in which the WSS filtered the CUT RX signal with different optical bandwidths $B_{WSS} = [52.0, 62.4, 72.8, 83.2]$ GHz.

For each considered scenario, 200 different WDM channel configurations were measured, by varying all the parameters of the LIC and the RIC, according to LHS, in an scenario equiva-

[3]Specifically, $B_{WSS} > R_s(1+\rho) + G_{L/R,max}/2$.

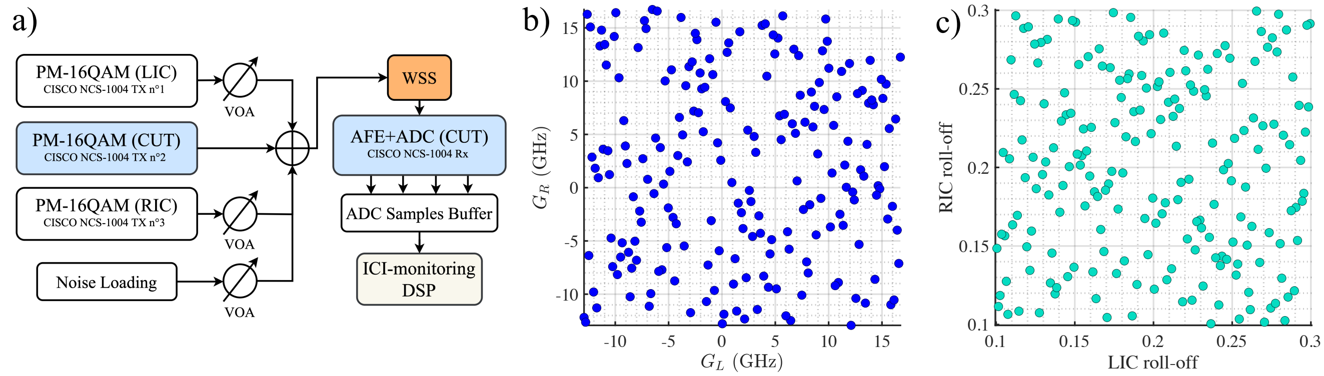


**Fig. 10.** a) Experimental Setup; b,c) Experimental LHS distribution for guard-band and roll-off values. AFE: Analog Front-End

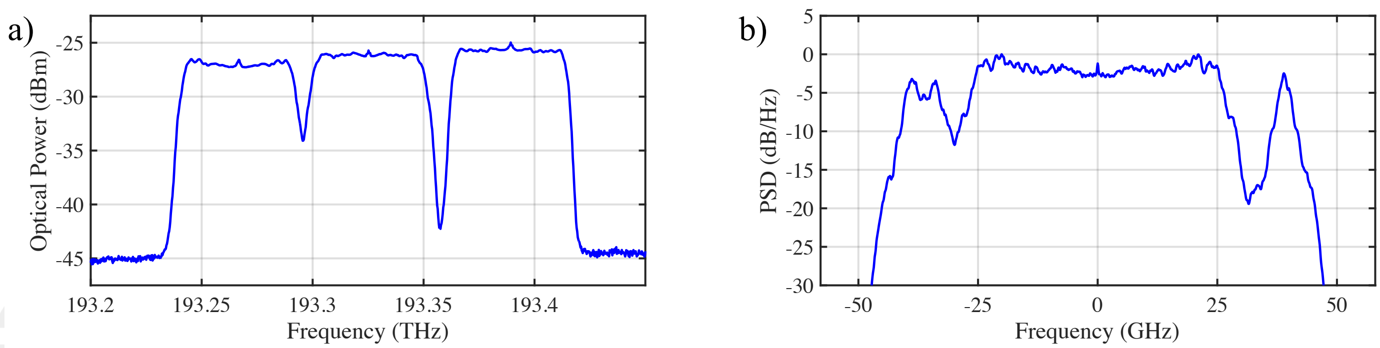


**Fig. 11.** Power spectral density measurement on the experimental setup through a) Optical Spectrum Analyzer acquisition; b) dual-polarization PSD computation using RX ADC samples, acquired from the commercial coherent transceiver. In the illustrated configuration: $G_L$=-3.2405 GHz, $G_R$=2.4215 GHz, $\rho_L$=0.1635, $\rho_R$=0.1165, $\alpha$=0.1775. No WSS was applied.



lent to the simulation Case #5. Due to practical constraints (i.e., limited granularity in the available commercial cards symbol rates), only the roll-off and the power of the LIC and RIC were varied through LHS across the configurations. Nevertheless, as observed in Sec. 3.B, interfering channels with variable roll-off values are equivalent to those with flexible symbol rates within the CUT spectrum (leading also to equivalent performance for our algorithm, as shown in Fig. 7). Therefore, the experimental results shown in this section can generalize also for a more generic assumption on the LIC and RIC spectral shape. Specifically, for each configuration, the CUT was a 52 Gbaud PM-16QAM modulated sequence, shaped to a root-raised-cosine spectrum with a fixed roll-off equal to 0.2. The LIC and RIC shared the same shaping and symbol rate as the CUT, but with roll-off varying from 0.1 to 0.3 (as in simulations). Consistent with the simulative case, the relative power of the interferers was varied between -3 dB and + 3dB with respect to the CUT power. However, due to practical limitations in the experimental setup, the total received power was kept constant. Therefore, instead of varying both $P_L$ and $P_R$, a relative power variation factor $\alpha = P_L/P_R$ was adjusted according to LHS. Finally, the guard-band values for both LIC and RIC were varied from -13 GHz to 16.5 GHz: as an example, Fig. 10(b) illustrates the different values of guard-band and roll-off of the RIC and the LIC used in the experiment after sampling through LHS (together with the $\alpha$ parameter, not shown in the Figure). In alignment with simulations, for each configuration, we captured a single acquisition of $2^{17}$ consecutive ADC samples (X/Y polarization and I/Q phase) from the coherent RX relative to the CUT (ADC sampling frequency $f_{ADC} = 96$ GHz). Figure 11 shows an example of optical spectrum measured on the experimental setup, using alternatively an OSA (Fig. 11(a)) or the RX ADC samples from the commercial receiver (Fig. 11(b)). To optimize and test the algorithm in the experiments, the ANN of the DSP scheme was trained using the same procedure and hyperparameters adopted in the simulative cases (refer to Sec. 3.A)

### B. Experimental results

The results obtained over the experimental setup previously described are depicted in Fig.12 and 13 , illustrating the estimation outcomes for both left and right guard-bands across various WSS filtering values (including no WSS filtering). The experimental performance of the ANN-based DSP scheme is first presented by means of scatter plots, illustrating for both the left (Fig.12(a)) and right (Fig.12(b)) guard-bands the distribution of the algorithm estimations as function of the true values. It is clear from the figures that, without optical filtering (green dots), the estimates of the algorithm precisely follow the true guard-band values, with a consistent performance across the entire guard-band range. Conversely, when the WSS is applied (violet dots, with estimated $B_{WSS} = 62.4$ GHz), the algorithm is accurate until the guard-band value is not relative to interfering channels entirely filtered out by the WSS: in that case, as no useful information can be retrieved from the CUT RX spectrum, the ANN provides a roughly constant guard-band estimate around 10 GHz, as a consequence of the minimum mean square error criterion adopted during the training.

Subsequently, as done for the simulations, Figs.13(a) and 13(b)

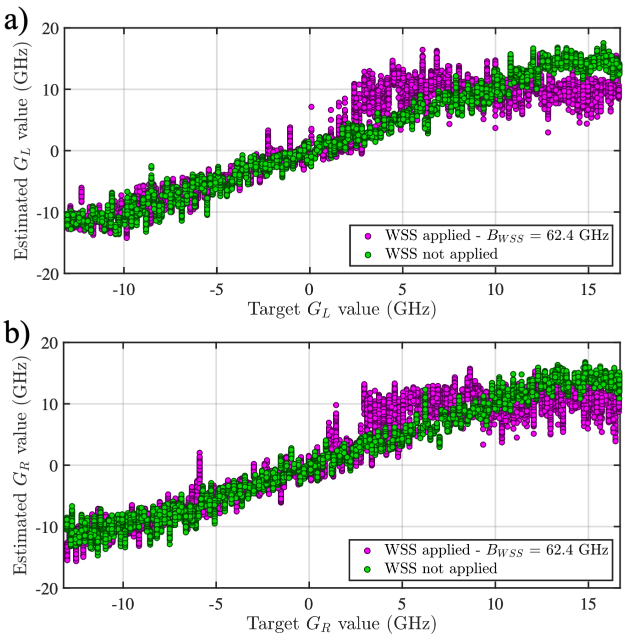


**Fig. 12.** Experimental results. Estimated guard-band as a function of the real guard-band for the LIC (a) and RIC (b), without optical filtering (purple tots) and with $B_{\text{WSS}} = 62.4$ GHz (green dots).

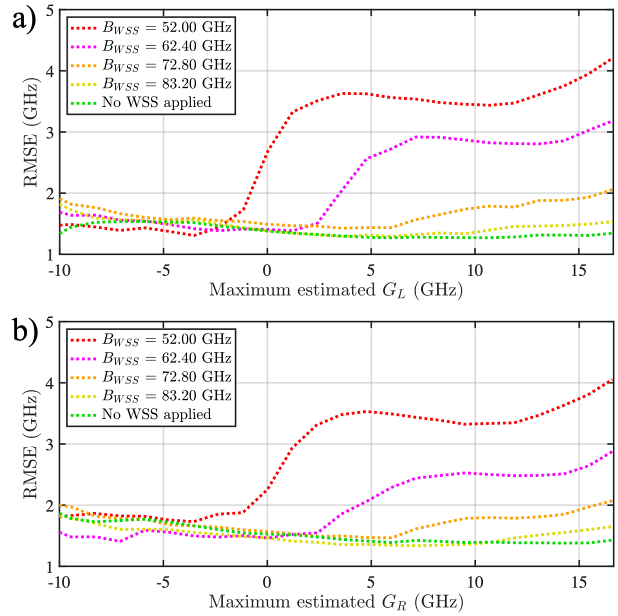


**Fig. 13.** Experimental results. RMSE of the guard-band estimation for the LIC (a) and RIC (b) as a function of the maximum guard-band at different values of optical filtering.



illustrate the evolution of the guard-band estimation RMSE in relation to the maximum estimated guard-band. The experimental results clearly show an evolution consistent to what observed in simulations: in all the considered scenarios, the algorithm provides accurate estimations of the guard-band, as long as the spectrum of the interfering channels is not erased by optical filtering (i.e., the WSS).

Finally, Fig.14 shows the overall RMSE across all the guard-bands as a function of the WSS bandwidth $B_{\text{WSS}}$. As observed in the simulative analysis, the algorithm overall performance is directly affected by the optical filtering applied to the receiver: when the WSS bandwidth decreases, so does the accuracy of the guard-band estimation. Nevertheless, the estimation RMSE equal to 1.5 GHz (corresponding to less than 3% of the CUT symbol rate) can be achieved either without optical filtering or with a large WSS bandwidth (i.e., $B_{\text{WSS}} = 83.2$ GHz). In summary, the experimental results closely replicate the simulation results, thus validating the proposed algorithm.

## 5. DISCUSSION AND CONCLUSION

In this paper, we proposed an algorithm that is capable of estimating the guard-band (i.e. the spectral distance) between neighboring WDM channels in a wavelength-routed optical network. The algorithm is based on applying an ANN-based digital signal processing scheme to raw samples captured by the ADC of a coherent receiver. This scheme can be either implemented off-line or integrated in the standard DSP chain. The information about the guard-band between a given channel under test and its interfering channels can be used to increase its symbol rate, thus incrementing the throughput and improving the overall efficiency of the network. The algorithm and its accuracy were tested through an extensive simulation analysis and subsequently validated through experimental results.

The presented research work also highlighted the main limitations of the proposed approach. The first, obvious limitation is the analog bandwidth of the receiver, which can limit the symbol rate maximization and, consequently, the utility of the guard-band estimation. The second limitation is the ADC sampling rate of the receiver: in fact, the algorithm is only able estimate guard-bands relative to interfering channels whose spectrum is at least partially present within the RX digital signal spectral range (e.g., $[-R_s, +R_s]$ using 2-SPS ADC samples). Nevertheless, a limited ADC sampling frequency at the RX side also limits the maximum achievable symbol rate of the CUT: therefore, estimating guard-bands exceeding the signal spectral range would be not beneficial for increasing the CUT throughput. The third limitation, demonstrated in both simulations and experiments, is the algorithm performance dependence on optical filtering effects generated throughout the network (i.e. induced by WSSs in the ROADMs). In this scenario, tight filtering limits the maximum detectable guard-band. Nevertheless, guard-bands that are too large compared to the available optical bandwidth are of little practical interest, since the symbol rate of the CUT is limited by the optical filtering. More importantly, smaller guard-bands can still be accurately estimated, albeit with a small performance penalty compared to the ideal case without filtering. Moreover, the effects of optical filtering on the algorithm appear to be independent of the number of possible cascaded ROADMs involved in CUT propagation: the limited guard-band range is primarily determined by the rectangular bandwidth $B_{\text{WSS}}$, which does not change either using a single or multiple WSSs [30]. The final limitation is related to the degree of knowledge of the parameters (e.g. symbol rate, roll-off and relative optical power) of the interfering channels. As demonstrated in the simulations, any uncertainty regarding these parameters will inevitably increase the estimation error of the guard-band, ranging from 0.8% (all parameters known) up to 2.3% (all parameters unknown) of the CUT symbol rate.

In conclusion, the simulative and experimental results presented in this manuscript demonstrate that, given an acceptable level of estimation accuracy for the specific network require-

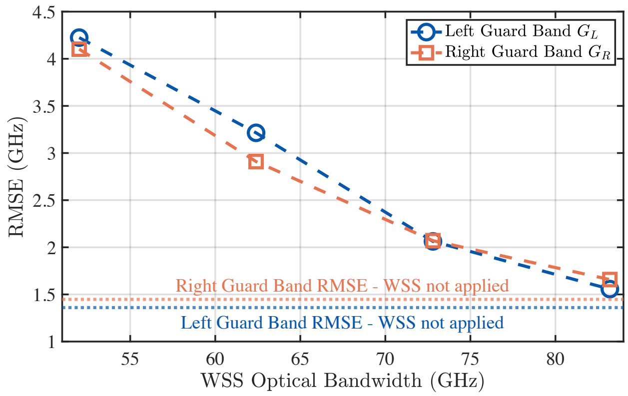


**Fig. 14.** Experimental results, measured as average RMSE for the guard-band estimation as a function of the WSS bandwidth.

ments, the proposed ANN-based DSP algorithm has the potential to serve as a solution for monitoring inter-channel interference in flexible wavelength-routed networks.

## FUNDING

This work was carried out under a Sponsored Research Agreement (SRA) with Cisco Photonics Italy S.r.l.. It was also partially sponsored by the European Union under the Italian National Recovery and Resilience Plan (NRRP) of NextGenerationEU, partnership on 'Telecommunications of the Future' (PE00000001 - program 'RESTART').

## ACKNOWLEDGMENTS

Portions of this work were presented at the OFC 2024 conference, paper W2A.32.

## REFERENCES

1. P. J. Winzer, D. T. Neilson, and A. R. Chraplyvy, "Fiber-optic transmission and networking: the previous 20 and the next 20 years [invited]," Opt. Express **26**, 24190–24239 (2018).
2. W. Klaus, P. J. Winzer, and K. Nakajima, "The role of parallelism in the evolution of optical fiber communication systems," Proc. IEEE **110**, 1619–1654 (2022).
3. P. J. Winzer, "The future of communications is massively parallel," J. Opt. Commun. Netw. **15**, 783–787 (2023).
4. T. Hoshida, V. Curri, L. Galdino, D. T. Neilson, W. Forysiak, J. K. Fischer, T. Kato, and P. Poggiolini, "Ultrawideband systems and networks: Beyond C+L-band," Proc. IEEE **110**, 1725–1741 (2022).
5. A. Ferrari, A. Napoli, J. K. Fischer, N. Costa, A. D'Amico, J. ao Pedro, W. Forysiak, E. Pincemin, A. Lord, A. Stavdas, J. P. F.-P. Gimenez, G. Roelkens, N. Calabretta, S. Abrate, B. Sommerkorn-Krombholz, and V. Curri, "Assessment on the achievable throughput of multi-band ITU-T G.652.D fiber transmission systems," J. Light. Technol. **38**, 4279–4291 (2020).
6. J. Cho and P. J. Winzer, "Probabilistic constellation shaping for optical fiber communications," J. Light. Technol. **37**, 1590–1607 (2019).
7. T. Zami, B. Lavigne, I. F. de Jauregui Ruiz, M. Bertolini, Y.-H. C. Kao, O. B. Pardo, M. Lefrançois, F. Pulka, S. Chandrasekhar, J. Cho, X. Chen, D. Che, E. Burrows, P. Winzer, J. Pesic, and N. Rossi, "Simple self-optimization of wdm networks based on probabilistic constellation shaping [invited]," J. Opt. Commun. Netw. **12**, A82–A94 (2020).
8. M. Shtaif, C. Antonelli, A. Mecozzi, and X. Chen, "Challenges in estimating the information capacity of the fiber-optic channel," Proc. IEEE **110**, 1655–1678 (2022).
9. A. Lord, S. J. Savory, M. Tornatore, and A. Mitra, "Flexible technologies to increase optical network capacity," Proc. IEEE **110**, 1714–1724 (2022).
10. S. Searcy, T. Richter, S. Burtsev, and S. Tibuleac, "Benefits of quasi-continuous symbol rate tunability in links constrained by ROADM filtering," J. Opt. Commun. Netw. **14**, C50–C56 (2022).
11. O. Ayoub, O. Karandin, M. Ibrahimi, A. Castoldi, F. Musumeci, and M. Tornatore, "Tutorial on filterless optical networks [invited]," J. Opt. Commun. Netw. **14**, 1–15 (2022).
12. E. Riccardi, P. Gunning, Óscar González de Dios, M. Quagliotti, V. López, and A. Lord, "An operator view on the introduction of white boxes into optical networks," J. Light. Technol. **36**, 3062–3072 (2018).
13. D. Pilori, A. Nespola, F. Forghieri, S. Piciaccia, and G. Bosco, "Real-time monitoring of the impact of cascaded wavelength-selective switches in digital coherent receivers," in *Conference on Lasers and Electro-Optics,* (Optica Publishing Group, 2020), p. SW3L.2.
14. A. E. Pérez, O. D. Vargas Bonett, S. E. Ralph, and J. J. Granada Torres, "Spectral spacing estimation in gridless Nyquist-WDM systems using local binary patterns," in *2021 IEEE Photonics Conference (IPC),* (2021), pp. 1–2.
15. N. P. Puentes, A. E. Pérez, and J. J. G. Torres, "Deep learning approach to estimate interchannel interference in gridless Nyquist-WDM systems," in *Frontiers in Optics + Laser Science 2022 (FIO, LS),* (Optica Publishing Group, 2022), p. JW5B.55.
16. A. Hraghi, L. Minelli, A. Nespola, S. Piciaccia, and G. Bosco, "Experimental demonstration of linear inter-channel interference estimation based on neural networks," IEEE Photonics J. **15**, 1–6 (2023).
17. L. Minelli, G. Bosco, A. Nespola, S. Straullu, S. Piciaccia, and D. Pilori, "Efficient inter-channel interference monitoring using DSP in standard coherent receivers," in *Optical Fiber Communication Conference (OFC) 2024,* (Optica Publishing Group, 2024), p. W2A.32.
18. H. Sun and K.-T. Wu, *Timing Synchronization in Coherent Optical Transmission Systems* (John Wiley & Sons, Ltd, 2016), chap. 10, pp. 355–394.
19. J. Pan and S. Tibuleac, "Real-time ROADM filtering penalty characterization and generalized precompensation for flexible grid networks," IEEE Photonics J. **9**, 1–10 (2017).
20. A. Jain and J. C. Cartledge, "Analysis of bandwidth narrowing in wavelength selective switch enabled DP-64QAM systems with transceiver noise," J. Light. Technol. **41**, 4590–4597 (2023).
21. P. A. Loureiro, A. Lorences-Riesgo, S. Mumtaz, M. S. Neves, D. L. Gac, T.-H. Nguyen, Y. Frignac, Y. Zhao, P. P. Monteiro, G. Charlet, S. Dris, and F. P. Guiomar, "On the mitigation of WSS filtering penalties: Single- vs multi-carrier modulation," J. Light. Technol. **41**, 3628–3634 (2023).
22. K. Kikuchi, "Fundamentals of coherent optical fiber communications," J. Light. Technol. **34**, 157–179 (2016).
23. P. Stoica and R. L. Moses, *Spectral analysis of signals*, vol. 452 (Pearson Prentice Hall, 2005).
24. X. Zhou and C. Xie, *Enabling technologies for high spectral-efficiency coherent optical communication networks* (John Wiley & Sons, 2016).
25. D. Godard, "Passband timing recovery in an all-digital modem receiver," IEEE Trans. on Commun. **26**, 517–523 (1978).
26. X. Dong, L. Liu, K. Musial, and B. Gabrys, "Nats-bench: Benchmarking nas algorithms for architecture topology and size," IEEE transactions on pattern analysis machine intelligence **44**, 3634–3646 (2021).
27. M. Stone, "Cross-validation: A review," Stat. A J. Theor. Appl. Stat. **9**, 127–139 (1978).
28. M. D. Mckay, R. J. Beckman, and W. J. Conover, "A comparison of three methods for selecting values of input variables in the analysis of output from a computer code," Technometrics **42**, 55–61 (2000).
29. K. Burrage, P. Burrage, D. Donovan, and B. Thompson, "Populations of models, experimental designs and coverage of parameter space by latin hypercube and orthogonal sampling," Procedia Comput. Sci. **51**, 1762–1771 (2015).
30. C. Pulikkaseril, L. A. Stewart, M. A. F. Roelens, G. W. Baxter, S. Poole, and S. Frisken, "Spectral modeling of channel band shapes in wavelength selective switches," Opt. Express **19**, 8458–8470 (2011).